ELSEVIER

Physica E 4 (1999) 1–10

PHYSICA E

Ground and excited states of few-electron systems in spherical quantum dots

B. Szafran, J. Adamowski *, S. Bednarek

Faculty of Physics and Nuclear Techniques, Technical University (AGH), al. Mickiewicza 30, 30059 Kraków, Poland

Received 31 August 1998; accepted 30 September 1998

Abstract

Energy spectra of two- and three-electron systems confined in semiconductor quantum dots, i.e., artificial helium and lithium atoms, are studied by the variational method under the assumption of the spherically symmetric confinement potential of finite depth. It is shown that the electron pairs and triples can form bound states if the quantum 'capacity', V_0R^2, of the quantum dot, is sufficiently large (V_0 is the potential-well depth and R is the quantum-dot radius). The conditions of binding have been determined for the ground and excited states. The binding energy and dipole transition energy have been calculated for several QDs. It is found that the dipole transition energy for the one-, two-, and three-electron artificial atoms is nearly independent of the number of electrons.

PACS: 73.20.Dx

Keywords: Semiconductor nanostructures; Quantum dots; Artificial atom

1. Introduction

Excess electrons introduced into a semiconductor quantum dot (QD) are subjected to a three-dimensional confinement potential, which results from potential barriers at the boundaries and/or the external voltage applied [1,38,39]. The depth and range of the confinement potential can be changed intentionally, which yields an energy spectrum with the designed properties. The QD with the confined electrons can be treated as an artificial atom [2,3]. The QD nanocrystals of nearly spherical shape embedded in an insulating matrix have been fabricated from the group IV semiconductors [4,5] and from the semiconducting compounds II–VI, III–V [6,40], I–VII [7,41], and IV–VI [8].

Theoretical description of electron states in QDs was a subject of papers [2,9–19]. The authors of these papers assumed infinitely deep confinement potentials, which possessed exclusively the bound states. This was either the rectangular potential well of infinite depth [9] or the parabolic potential [2,10–19]. The ground-state energy of few-electron QDs with the confinement potential of finite depth was studied by Fong et al. [20] with the help of the local-density approximation. When using the confinement potential of infinite depth, the following fundamental physical

* Corresponding author. Tel.: +48 12 6172974; fax: +48 12 6340010; e-mail: adamowski@novell.ftj.agh.edu.pl.

1386-9477/99/$ – see front matter
PII: S1386-9477(98)00247-1

problem arises: a continuum-energy threshold does not exist and the excess electrons are always bound by the confinement potential, i.e., possess only discrete energy levels. Therefore, the binding and dissociation processes cannot be described. This problem can be solved if we introduce the confinement potential of finite depth, which moreover much better describes the real QD-nanostructure, since the potential confining the electrons always possesses the finite depth and range. Moreover, the application of the finite confinement potential allows us to determine the quantum 'capacity' of the dot, i.e., to predict the number of electrons, which can be added to a QD in a given quantum state.

The subject of the present paper is closely connected with the problem of electron states in porous silicon [21,22]. It is suggested [21,22] that the emission of visible light from the porous silicon results from the electron and hole states confined in Si nanocrystals. It was found [21,22] that the effective-mass model with finite barriers fairly well accounts for the properties of porous silicon.

In the present work we investigate the possibility of formation of bound states of two- and three-electron systems confined in spherical QDs. The application of the confinement potential of finite depth allows us to give a clear physical interpretation for the binding of electrons in the QD and to determine the quantum 'capacity' of the QD. Preliminary results for the two-electron QDs were announced in Ref. [23]. Using the finite confinement potential, we [24,25] demonstrated that the excited states of D^- donor centers can be bound in spherical QDs.

The paper is organized as follows: the theoretical model is presented in Section 2, the problem of electron–electron correlation is discussed in Section 3, the results of calculations are given in Section 4, the conclusions and the discussion of an applicability of the present results to a description of experiments are contained in Section 5, and the results of the paper are summarized in Section 6.

2. Theory

We consider a system of few excess electrons confined in a single spherical semiconductor QD, which forms a potential-well region and is embedded in an insulating material (potential-barrier region). The confinement potential is assumed in a form of the spherical potential well, i.e., $V(r) = -V_0$ for $r < R$ and $V(r) = 0$ for $r > R$, where R is the radius of the QD, V_0 is the depth of the potential well, and $V_0 > 0$. The energy of the conduction-band minimum of the barrier material is set equal to zero and taken as the reference energy. Such choice of the reference energy allows us to separate the discrete energy levels of the electrons in the QD, which result from the size quantization, from the quasi-continuous energy of the conduction-band electrons in the barrier region. In the effective mass approximation, the Hamiltonian of the system of N electrons in the QD has the form

$$H = \sum_{i=1}^{N} [-\nabla_i^2 + V(r_i)] + \sum_{i=1}^{N} \sum_{j>i}^{N} \frac{2}{r_{ij}}, \tag{1}$$

where $r_{ij} = |\boldsymbol{r}_i - \boldsymbol{r}_j|$, $\boldsymbol{r}_i$ are the position vectors of electrons, the donor Rydberg $R_D = m_e \kappa^2 e^4 / 2\hbar^2 \varepsilon_s^2$ is the unit of energy, the donor Bohr radius $a_D = \varepsilon_s \hbar^2 / m_e \kappa e^2$ is the unit of length, $\kappa = 1/4\pi\varepsilon_0$, and ε_0 is the permittivity of vacuum. The changes of the electron effective band mass m_e and static dielectric constant ε_s at the QD boundary are neglected.

We have solved the eigenvalue problem for Hamiltonian (1) by the variational method with the trial wave function, which is built from the wave functions of one-electon states for the spherical potential well. These one-electron wave functions have been taken on as linear combinations of Slater-type orbitals, which reproduce the subsequent one-electron energy levels with a large accuracy [25]. Under the assumption of the Russell–Saunders coupling, the total spin and total orbital angular momentum of the electrons are well defined. The proposed trial wave function has the following form:

$$\Psi_v^{\mathrm{I}}(\{\xi_i\}) = \sum_{\{n_i\}} c_{v\{n_i\}} \psi_{v\{n_i\}}(\{\xi_i\}), \tag{2}$$

where $\xi_i = (\boldsymbol{r}_i, \sigma_i)$, $\{\xi_i\} = (\xi_1, \ldots, \xi_N)$ denotes the set of the position vectors $\boldsymbol{r}_i$ and spin variables σ_i, and $c_{v\{n_i\}}$ are the linear variational parameters ($i = 1, \ldots, N$). Basis wave functions $\psi_{v\{n_i\}}$ in Eq. (2) are proposed as properly symmetrized linear combinations of Slater determinants, that are constructed from the one-electron orbitals of the form

$$\varphi_{n_i lm}^{v}(\boldsymbol{r}) = r^{n_i} \exp(-\gamma_v r) Y_{lm}(\theta, \phi), \tag{3}$$

where γ_v are the nonlinear variational parameters and $Y_{lm}(\theta,\phi)$ are the spherical harmonics. In the present calculations, the parameters $\{n_i\}=(n_1,n_2,n_3)$ take on the values $n_i=0,\ldots,12$.

We consider the following two-electron states: $(1s^2)\ ^1S$, $(1s1p)\ ^1P$, $(1s1p)\ ^3P$, $(1p^2)\ ^3P$, $(1p^2)\ ^1D$, $(1p^2)\ ^1S$, $(1s1d)\ ^1D$, $(1s1d)\ ^3D$, $(1s2s)\ ^1S$, and $(1s2s)\ ^3S$, and three-electron states: $(1s^21p)\ ^2P$, $(1s1p^2)\ ^4P$, $(1s^21d)\ ^2D$, $(1s^22s)\ ^2S$, and $(1s1p^2)\ ^2S$. The symbols in parentheses denote the occupation of the one-electron orbitals, the capital letters S, P, and D correspond to the total angular-momentum quantum numbers $L=0,1$, and 2, respectively, and the superscripts outside the parentheses – the total-spin multiplets. Below, we give the two exemplary basis functions:

$$\psi^{v}_{n_1n_2}(\xi_1,\xi_2)=\mathscr{A}[\varphi^{v}_{n_100}(\boldsymbol{r}_1)\alpha(\sigma_1)\varphi^{v}_{n_200}(\boldsymbol{r}_2)\beta(\sigma_2)] -\mathscr{A}[\varphi^{v}_{n_100}(\boldsymbol{r}_1)\beta(\sigma_1)\varphi^{v}_{n_200}(\boldsymbol{r}_2)\alpha(\sigma_2)] \tag{4}$$

for the two-electron state $v=(1s^2)\ ^1S$ and

$$\psi^{v}_{n_1n_2n_3}(\xi_1,\xi_2,\xi_3) =\mathscr{A}[\varphi^{v}_{n_100}(\boldsymbol{r}_1)\alpha(\sigma_1)\varphi^{v}_{n_200}(\boldsymbol{r}_2)\beta(\sigma_2)\varphi^{v}_{n_310}(\boldsymbol{r}_3)\alpha(\sigma_3)] -\mathscr{A}[\varphi^{v}_{n_100}(\boldsymbol{r}_1)\beta(\sigma_1)\varphi^{v}_{n_200}(\boldsymbol{r}_2)\alpha(\sigma_2)\varphi^{v}_{n_310}(\boldsymbol{r}_3) \times\alpha(\sigma_3)] \tag{5}$$

for the three-electron state $v=(1s^21p)\ ^2P$, where $\mathscr{A}$ is the antisymmetrization operator, $\alpha(\sigma)$ and $\beta(\sigma)$ are the spinors. The basis wave functions for the other considered states have been constructed in a similar manner. We took on various numbers of terms in expansion (2), which ensured the necessary accuracy of the calculations. The shortest expansion included 91 terms for two-electron state $(1s^2)\ ^1S$ and the longest – 364 terms for three-electron state $(1s^21p)\ ^2P$.

3. Electron–electron correlation

The exact wave function of the few-electron system should take into account the electron–electron correlation. The correlation can be included in a twofold manner [26]. One can propose the variational wave function, which either explicitly depends on the relative positions of electrons or implicitly includes this dependence in an expansion into many Slater determinants corresponding to the excited states. This second approach is called the configuration-interaction (CI) method [26]. In the present work, we have applied both the approaches. For the two-electron systems, we can introduce the explicit dependence on the electron–electron separation as follows [25]:

$$\Psi^{\Pi}_{v}(\boldsymbol{r}_1,\boldsymbol{r}_2)=\exp[-\alpha_v(r_1+r_2)]\sum_{mnp}c^{v}_{mnp} \times(1\pm\mathscr{P}_{12})r_1^m r_2^n r_{12}^p P_L(\cos\theta_1). \tag{6}$$

The considered state v is characterized by the total angular-momentum quantum number L and corresponds to either the spin singlet (sign $+$) or spin triplet (sign $-$). In Eq. (6), $\mathscr{P}_{12}$ is the permutation operator, which interchanges the electron indices, i.e., $1\rightleftharpoons 2$, α_v and c^{v}_{mnp} are the variational parameters, $P_L(\cos\theta_i)$ is the Legendre polynomial of order L, and θ_i is the angle between z-axis and vector $\boldsymbol{r}_i$, the sum over p includes the terms with $p=0$ and 1, which enables us to calculate all the matrix elements analytically, and the other sums run over the integral values of m and n from the interval $[0,\ldots,12]$, which are chosen so that the proper symmetry of the wave function is ensured [25]. Wave function (6) was checked [25] to be sufficiently flexible both for the H^- ion and He atom in an infinite space and for the H^- ion confined in a spherical cavity. Its one-electron version very well reproduces the known analytical solutions for one-electron problems in the spherical potential well [25]. In the present work, we apply wave function (6) to test calculations mainly, since – as we will show – the results obtained with the use of trial wave function (2) only slightly differ from those obtained with Eq. (6).

Trial wave function (2), introduced in Section 2, also takes into account the electron–electron correlation in accordance with the method of configuration interaction [26]. However, the correlation is included only partially, since not all one-electron excited states are used in the construction of wave function (2). The correlation would be fully included if we used all the one-electron orbitals, that form the total wave function of the required symmetry.

Fig. 1 shows the ground-state energy of two electrons in the QD calculated with the use of wave

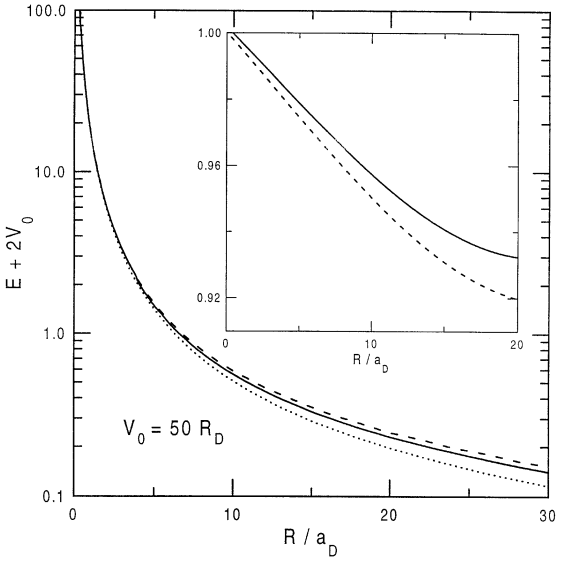

Fig. 1. Ground-state energy of the two-electron system in the QD with $V_0 = 50R_D$ as a function of QD radius. Solid curve shows the results obtained with the use of wave function (2), dotted curve – with Eq. (6), and dashed curve – by the Hartree–Fock method. The donor Rydberg R_D is the unit of energy and the donor Bohr radius a_D is the unit of length. The energy is determined with respect to the twice conduction-band minimum of the potential-well region. Inset: Overlap of wave function (2) (solid curve) and Hartree–Fock wave function (dashed curve) with wave function (6) for two electrons.

functions (2) and (6). The results obtained with wave function (6) can be regarded to be 'exact' [25]. For comparison, we have also performed the calculations by the Hartree–Fock method with the wave function being a single Slater determinant. In the Hartree–Fock method the correlation is fully neglected. The results obtained (Fig. 1) with trial wave function (2) and by the Hartree–Fock method are almost indistinguishable from the 'exact' results for the QDs of small and intermediate size, i.e., in strong- and intermediate-confinement regimes [27]. The differences are visible for large QDs, i.e., in a weak-confinement regime [27]. The limit $R \to \infty$ corresponds to the electron gas, for which the correlation provides a considerable contribution to the ground-state energy. The inset of Fig. 1 shows the calculated overlaps of wave function (2) and the Hartree–Fock wave function with the 'exact' wave function (6), which allows us to estimate relative errors done when neglecting partially and fully the electron–electron correlation. We see that both the overlaps are close to 1 even for relatively large QDs. These results show that – in the strong- and intermediate-confinement regimes – the electron–electron correlation plays a minor role in QDs and can be properly described by the CI-type wave function (2). We can even fully neglect the correlation (cf. the Hartree–Fock results) and – in spite of this – obtain useful results. These test results together with the appropriate tests described in Ref. [25] provide quantitative arguments for the reliability of the results obtained with the use of variational wave function (2).

4. Results

We are interested in the binding of few-electron states in QDs. The condition of binding of N-electron state v with the energy $E_v^{(N)}$ has the form

$$E_v^{(N)} < E_{\mathrm{th}}^{(N)}, \tag{7}$$

where $E_{\mathrm{th}}^{(N)}$ is the continuum-threshold energy for the N-electron system. For the assumed reference energy, the continuum-threshold energy takes on the following values: $E_{\mathrm{th}}^{(1)} = 0$, i.e., the energy of the electron in the conduction-band bottom of the barrier material, $E_{\mathrm{th}}^{(2)} = E_{1s}^{(1)}$, i.e., the energy of the dissociated two-electron system with one electron bound in the 1s state and the second electron liberated to the conduction-band bottom of the barrier region, and $E_{\mathrm{th}}^{(3)} = E_0^{(2)}$, i.e., the energy of the dissociated three-electron system with two electrons bound in the ground state with the energy $E_0^{(2)}$ and the third electron liberated to the conduction-band bottom of the barrier region. The binding energy $W_v^{(N)}$ of the vth state of N-electron system is defined as

$$W_v^{(N)} = E_{\mathrm{th}}^{(N)} - E_v^{(N)}. \tag{8}$$

A fulfillment of condition of binding (7) is equivalent to the statement that the binding energy $W_v^{(N)}$ is positive.

The energy levels of the two- and three-electron artificial atoms calculated with the use of trial wave function (2) are shown in Figs. 2a, b and 3. The one-electron energy levels are also shown for comparison. The results depicted in Figs. 2a, b and 3 demonstrate that the few electrons confined in the QD can form bound states. Both the ground and excited

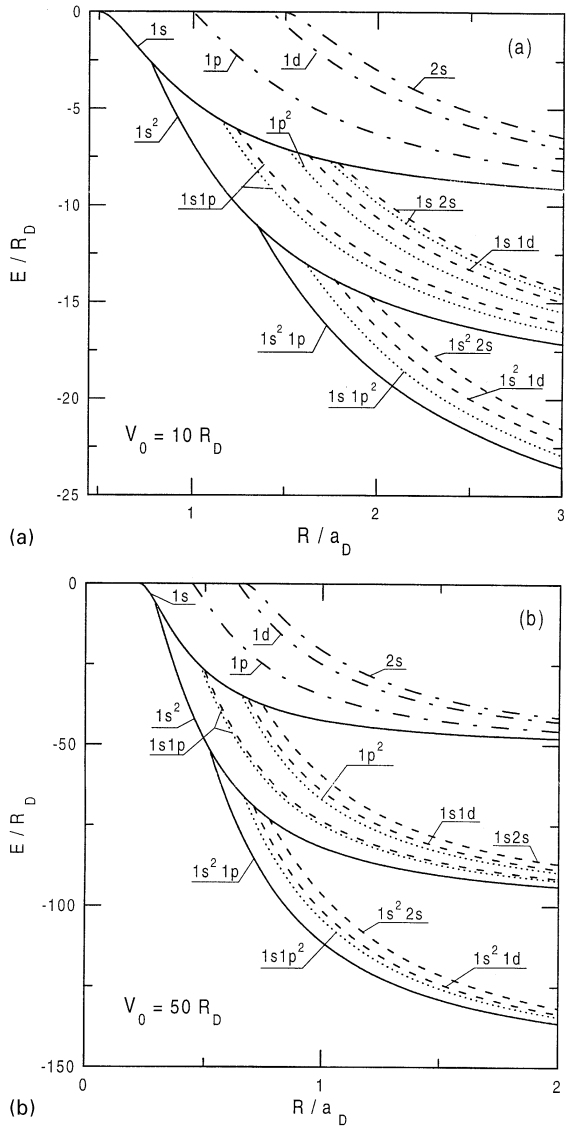

Fig. 2. Energy levels of one-, two-, and three-electron systems in spherical QD as functions of radius R for (a) $V_0 = 10R_D$ and (b) $V_0 = 50R_D$. Solid curves correspond to the ground states, dashed (dotted) – excited spin-unpolarized (polarized) states, and dash-dotted – excited one-electron states. The units are the same as in Fig. 1.

states can be bound if the QD radius is sufficiently large.

Figs. 2b and 3 display the results for the QDs with deep potential wells, which correspond to the nanostructures made of $GaAs/Al_{1-x}Ga_xAs$ with $x > \sim$ 0.3, Si/SiO_2, and Ge/SiO_2. The results in Fig. 2a show that even the QD with the relatively shallow potential well can bind electrons. The results of Fig. 2a can be applied to the $GaAs/Al_{1-x}Ga_xAs$ QDs with $x < \sim 0.1$. Figs. 2a, b and 3 show the energy levels of few-electron systems confined in the QDs of small and intermediate size, i.e., they correspond to the strong- and intermediate-confinement regimes [27]. In these QDs, the spin-singlet state $(1s^2)\ ^1S$ is the ground state of the electronic pair and the spin-doublet state $(1s^21p)\ ^2P$ is the ground state of the electronic triple.

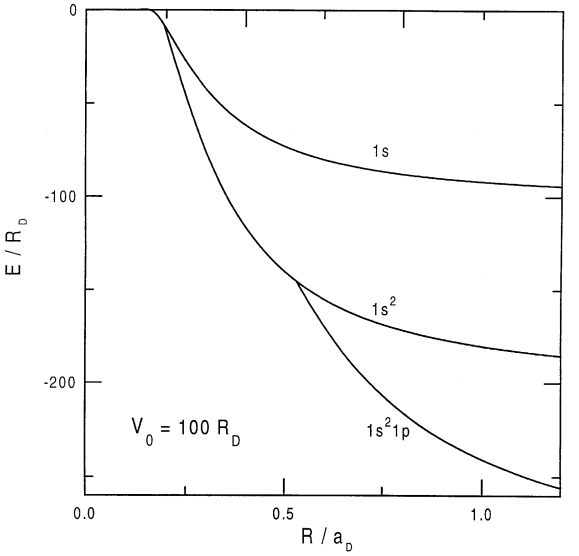

Fig. 3. Ground-state energy of one-, two-, and three-electron systems in spherical QD as a function of radius R for $V_0 = 100R_D$. The units are the same as in Fig. 1.

Fig. 3 displays only the ground-state energy levels. Moreover, in Fig. 2a and b some energy levels of the two-electron excited states are omitted, since they lie too close to the displayed levels. All the energy levels calculated for the electron pair are shown in Fig. 4 for the QDs of small $(R = 2a_D)$ and large $(R = 15a_D)$ size. Left and middle energy-level ladders show that the electron–electron interaction lifts the degeneracy of the energy levels, which are associated with the states of the different total spin and total orbital angular momentum. This splitting results from the Russell–Saunders coupling. The order of energy levels essentially changes if the size of the QD increases (cf. middle and right energy-level ladders). These results

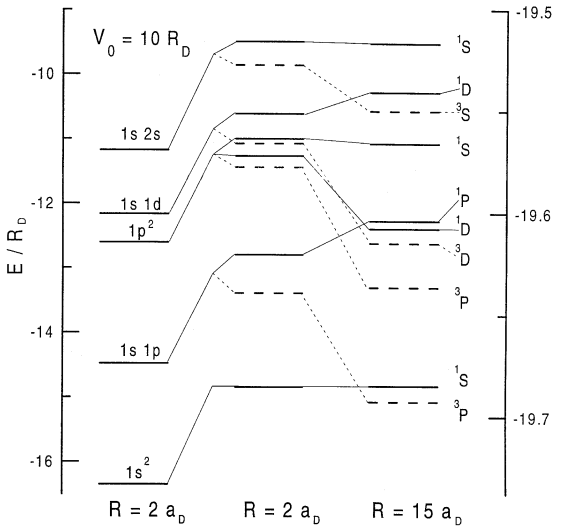

Fig. 4. Energy levels of electron pair in the QDs with $V_0 = 10R_D$ and the radius $R = 2a_D$ (left and middle parts, left energy scale) and $R = 15a_D$ (right part, right energy scale). Left energy-level ladder corresponds to the noninteracting electrons, middle and right – to the interacting electrons. Solid lines correspond to spin-singlet states and dashed – spin-triplet states. Thin lines show the correspondence between the energy levels.

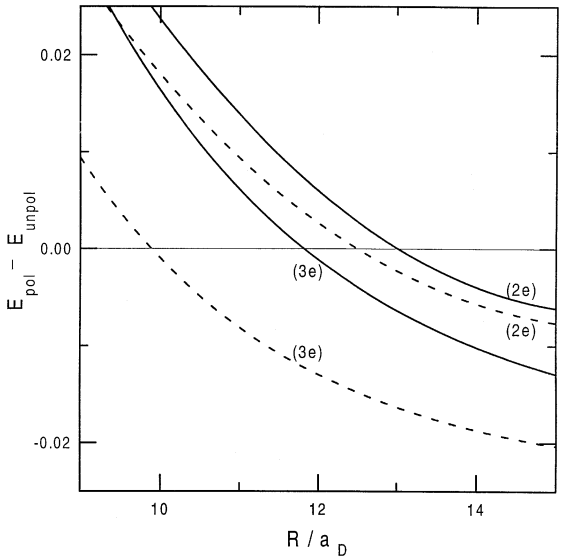

Fig. 5. Difference between the lowest energy levels associated with the spin-polarized (E_{pol}) and spin-unpolarized (E_{unpol}) states for the systems of two (2e) and three (3e) electrons in QDs as a function of radius R. States $(1s1p)^3P$ of (2e) and $(1s1p^2)^4P$ of (3e) are the spin-polarized states and $(1s^2)^1S$ of (2e) and $(1s^21p)^2P$ of (3e) are the spin-unpolarized states. Solid curves correspond to $V_0 = 50R_D$, dashed – $V_0 = 10R_D$. The units are the same as in Fig. 1.

express a general trend, according to which the triplet states substantially lower their energy and begin to be located below the energy levels of the corresponding singlet states if the QD radius is sufficiently large.

A 'phase transition' from the low-spin to high-spin ground state is shown in Fig. 5, which displays the energy difference between the levels associated with the spin-polarized and spin-unpolarized states. The states $(1s1p)\ ^3P$ and $(1s1p^2)\ ^4P$ are the spin-polarized states for the two and three electrons, respectively, and the states $(1s^2)\ ^1S$ and $(1s^21p)\ ^2P$ are the corresponding spin-unpolarized states. The dashed curve (2e) in Fig. 5 shows that – for the potential-well depth $V_0 = 10R_D$ – the ground state of the electron pair in the QD changes from the singlet to triplet at $R \simeq 12.5a_D$. The corresponding transformation of the three-electron ground state from the doublet to quadruplet occurs at $R \simeq 10a_D$ [dashed curve (3e)]. The critical values of the QD radius for the low–high spin ground-state transformation slowly increase with the increasing potential-barrier height (cf. the solid curves in Fig. 5 for $V_0 = 50R_D$). The singlet–triplet 'phase transition' occurs for a certain critical electron–electron separation, i.e., for a corresponding critical density. A similar density-induced phase transition is known from the theory of electron gas: according to the results obtained [28,42] by the Hartree–Fock method, the electron gas below the critical density goes over from the paramagnetic into ferromagnetic state.

The formation of the bound electron states is determined by both the depth and range of the confinement potential. In order to describe this effect we introduce the effective quantum 'capacity' of the QD defined as the product V_0R^2. The condition of binding [Eq. (7)] for the νth state of the N-electron system can be formulated in terms of the quantum capacity as follows:

$$V_0R^2 > \Omega_\nu^{(N)}, \tag{9}$$

which means that the considered state becomes bound if the effective 'capacity' of the QD exceeds the critical value $\Omega_\nu^{(N)}$. It is well known that the subsequent one-electron states in the spherical potential well are bound if the values of V_0R^2 (expressed in units $R_Da_D^2$) are larger than $\pi^2/4, \pi^2, 2\pi^2$, and $9\pi^2/4$ for the states

Table 1
Estimated critical values of the quantum 'capacity', V_0R^2, of the QD for the binding of the given two-electron states (in units $R_D a_D^2$). The values obtained from the simple 'sum rule' described in the text are listed in the third row

$(1s^2)^1S$	$(1s1p)^3P$	$(1s1d)^3D$	$(1s2s)^3S$	$(1p^2)^3P$
5.08	12.52	22.45	29.26	22.64
4.93	12.34	22.21	24.67	19.74

Table 2
Estimated critical values of the quantum 'capacity', V_0R^2, of the QD for the binding of the given three-electron states. The numbers are given in the same units and order as in Table 1

$(1s^21p)^2P$	$(1s1p^2)^4P$	$(1s^21d)^2D$	$(1s^22s)^2S$
17.75	25.32	30.06	38.03
14.80	22.21	24.67	27.14

1s, 1p, 1d, and 2s, respectively. We have determined the critical values of the quantum capacity of the QD for the binding of two-electron (Table 1) and three-electron (Table 2) artificial atoms. We have found that the following simple 'sum rule' is roughly fulfilled: the critical effective quantum capacity for the binding of the few-electron state is approximately equal to (or greater than) the sum of the critical effective capacities for the binding of the one-electron states, from which the given state is built, e.g., $\Omega^{(2)}_{1s^2} \simeq 2\Omega^{(1)}_{1s}$, $\Omega^{(2)}_{1s1p} \simeq \Omega^{(1)}_{1s} + \Omega^{(1)}_{1p}, \Omega^{(2)}_{1s1d} \simeq \Omega^{(1)}_{1s} + \Omega^{(1)}_{1d}$. The deviations from this rule – due to the electron–electron interaction – are rather small for the two-electron states of the lowest energy (cf. Table 1).

The results of the present paper can be used to determine the epxerimentally accessible radiative-transition energies. Fig. 6 shows the energies of the dipole allowed radiative transitions S–P and P–D for the one-, two-, and three-electron systems in QDs. The transition energies have been calculated for the following lowest-energy-states: the S-state is the 1s state for the one-electron artificial atom (1e), the $(1s^2)\ ^1S$ state for the two-electron artificial atom (2e), and the $(1s1p^2)\ ^2S$ state for the three-electron artificial atom (3e); the P-state is the 1p state for (1e), the $(1s1p)\ ^1P$ state for (2e), and the $(1s^21p)\ ^2P$ state for (3e); and the D-state is the 1d state for (1e), the $(1s1d)\ ^1D$ for (2e), and $(1s^21d)\ ^2D$ for (3e). In the considered transitions, only the single one-electron orbital is

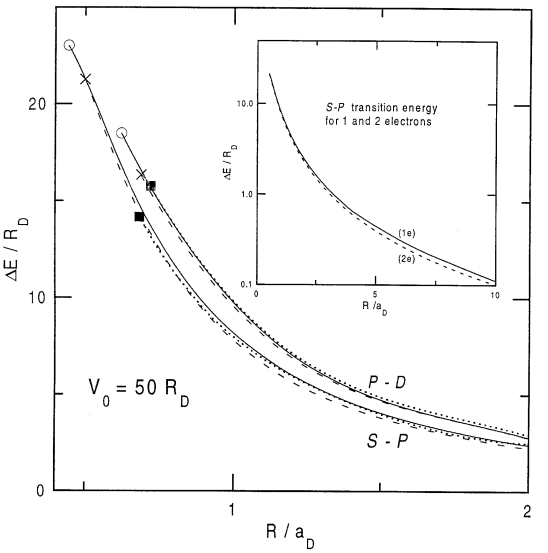

Fig. 6. Energy ΔE of radiative S–P and P–D transitions for the systems of one electron (solid curves), two electrons (dashed curves), and three electrons (dotted curves) in the QDs with $V_0 = 50R_D$ as functions of radius R. The symbols (circles, crosses, and squares) correspond to these values of R, at which the binding appears for the upper-energy state of the one, two, and three electrons, respectively. Inset: S–P transition energy for one (1e) and two (2e) electrons in the QDs of large radius.

changed. We see that – for the few-electron artificial atoms – the curves corresponding to the S–P and P–D radiative transitions are almost indistinguishable from each other. This means that these transition energies are nearly independent of the number of electrons in the QD, i.e., are independent of the electron–electron interaction. Until now, this property was known for electron systems in an external uniform magnetic field and two-dimensional parabolic confinement potential (generalized Kohn theorem [2,27]). The results of Fig. 6 show that this property is also valid for the few-electron systems in small QDs with the three-dimensional spherical confinement potential of finite depth. Inset of Fig. 6 points out that a certain dependence of the transition energy on the electron–electron interaction appears for QDs of large radius. However, in this case the values of both the transition energies and corresponding differences are very small.

We have also calculated average interparticle distances for the electronic pair (Fig. 7). The results of Fig. 7 provide information about the spatial

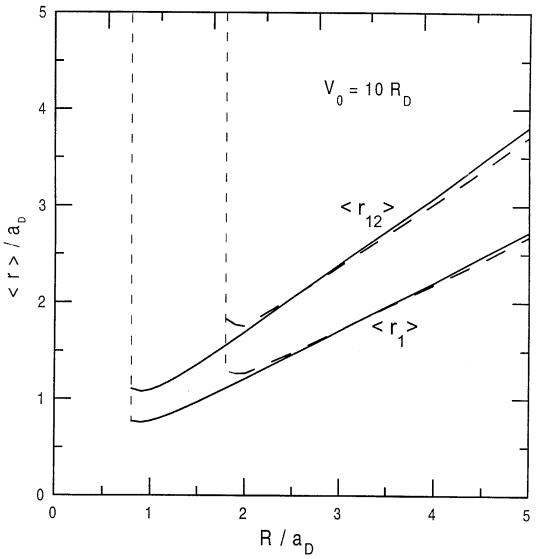

Fig. 7. Expectation values of electron–electron $\langle r_{12}\rangle$ and electron–dot center $\langle r_1\rangle$ distances for the two-electron ground state $(1s^2)^1S$ (solid curves) and excited state $(1s2s)^1S$ (dashed curves). The vertical dashed lines correspond to the unbound delocalized states. The donor Bohr radius a_D is the unit of length.

distribution of electrons in the QD. The expectation values of the electron–electron $\langle r_{12}\rangle$ and electron–dot center $\langle r_1\rangle$ distances for the states $(1s^2)\ ^1S$ and $(1s2s)\ ^1S$ increase almost linearly with the QD radius R, but are smaller than R. This means that the electrons in the bound state are spatially, almost completely, confined within the QD. The delocalization of the unbound states is shown by the dashed vertical lines. Fig. 7 also shows that – contrary to the natural helium atom – the interparticle distances in the artificial helium atom are nearly the same for the ground and excited states.

5. Discussion and conclusions

We have studied the properties of few-electron systems in spherical semiconductor QDs with the confinement potential of finite depth and range. The results obtained show that the bound states are created in the confined few-electron systems if the quantum capacity, i.e., V_0R^2, is sufficiently large. Based on these results, we predict that – even for the shallow confinement potential – the binding of few-electron states occurs for the QD of the relatively large size. The bound few-electron artificial atoms with size-quantized energy levels can be formed in large QDs with a rather small potential well depth [30]. The shallow confinement potential corresponds to $GaAs/Al_xGa_{1-x}As$ nanostructures with $x < \sim 0.1$. So far, the spherical QDs fabricated from GaAs were obtained only in an organic matrix [6]. No experimental data are known to us for artificial atoms in the spherical QDs fabricated from $GaAs/Al_xGa_{1-x}As$. In the cylindrical QDs made of $GaAs/Al_{0.22}Ga_{0.78}As/In_{0.05}Ga_{0.95}As$, the shell-filling effect in artificial atoms has been recently studied experimentally by the transport spectroscopy [31] and described theoretically by the present authors [32].

Table 3
Binding energy (W) of the ground state and S–P transition energy (ΔE) for the artificial atoms consisting of one (1e), two (2e), and three (3e) electrons in the nanocrystals of Si and Ge and in porous Si (p-Si). For p-Si, only the ground states of one and two electrons are bound in the Si nanocrystals of the estimated size [21]. The energy is expressed in meV

Nanocrystal	W(1e)	W(2e)	W(3e)	ΔE(1e)	ΔE(2e)	ΔE(3e)
Si	3156.0	3117.0	3025.0	45.29	45.03	45.61
Ge	3060.0	2858.0	2718.0	206.1	201.6	216.6
p-Si	512.7	298.1	–	–	–	–

The deep confinement potential is relevant to the Si/SiO_2 [4] and Ge/SiO_2 [5] nanostructures. In Table 3, we apply the present results to the QDs made of Si and Ge. The estimated radii of the nanocrystals are 5 nm for Si [4] and 1.6 nm for Ge [5]. We take on $R_D = 31.27$ and 9.81 meV and $a_D = 1.94$ and 4.58 nm for Si and Ge nanocrystals, respectively, and assume that the value $V_0 = 3.2$ eV estimated for Si/SiO_2 nanostructure [4] can as well be used for Ge/SiO_2. We also apply our results to the Si nanocrystals in the porous Si taking on $V_0 = 1.7$ eV [22] and $R = 1.25$ nm [21]. The results listed in Table 3 demonstrate that the binding energies of few-electron artificial atoms formed in Si and Ge spherical QDs are close to V_0 and the S–P transition energies are nearly equal to each other (cf. Fig. 6).

We remind the reader that the present theoretical model neglects the change of the electron band mass and dielectric constant at the QD boundary. The problem of space-dependent electron mass was considered by the present authors in Ref. [25] for one-electron states in spherical QDs. According to

Ref. [25] this effect is negligibly small for the large QDs with the deep confinement potential due to the vanishingly small penetration of electrons into the barrier region.

The change of the dielectric constant leads to the induced electric polarization at the QD boundary [33]. The influence of the electric polarization on the electron states in the spherical QD was studied in Refs. [33–35] under the assumption of the confinement potential of infinite depth. Based on these results [33–35], we can state that for the QD embedded in a dielectric medium of the smaller dielectric constant, which is the case of Si/SiO_2 and Ge/SiO_2 nanostructures, the electric polarization will contribute to an additional potential, which will repulse the electrons from the boundaries pushing them towards the dot center. As a result, the electrons will be more strongly localized inside the QD. For the heterostructures with the small difference of dielectric constants, e.g., GaAs/AlGaAs, the effect of electric polarization is small.

If the QD radius increases, the reordering of few-electron energy levels occurs. In particular, the spontaneous 'phase transition' appears from the low-spin in high-spin ground state. A similar behavior has been obtained by Bryant [9] for the infinite rectangular potential well and by Fujito et al. [16] and Müller and Koonin [17] for the parabolic potential. The singlet–triplet transition occurs in the natural He atom at high magnetic field.

The problem of spherical QDs was studied by Belkhir [36], who assumed that the electrons are constrained to move on the surface of the sphere of constant radius and applied the single-electron basis in order to diagonalize the Hamiltonian matrix. Since this constraint is essentially semiclassical, the author [36] found that the interaction energy for N-electron QD scales like $N(N-1)$, which is in agreement with the result of classical electrostatics for discrete charges. This effect was discussed in detail by Maksym et al. [37].

The dipole transition energy obtained in the present paper (Fig. 6) exhibits a similar property to that resulting from the generalized Kohn theorem [2,27,29,43,44] According to this theorem, the transition energy is independent of the electron–electron interaction, which holds true under the assumptions that the electrons are subjected to the external parabolic potential and the electron–photon interaction is described in the dipole approximation. This property results from the exact separation of the total Hamiltonian in the center-of-mass and relative coordinates of the electronic system [27]. The near independence of the S–P and P–D transition energies of the electron–electron interaction, found in the present paper, has a different reason. This property results from an approximate cancellation of the Coulomb interaction contributions to the lowest energy levels of electrons in the QD of small size and is connected with almost the same electron–electron separations in the ground and excited states (cf. Fig. 7). Therefore, in the spherical QDs of small radius, the major contribution to the transition energy stems from the differences between the one-electron energy levels of the potential well, which are nearly the same for one and many electrons. We note that the independence of the transition energy of the number of electrons, obtained in the present work, does not require the assumption of the dipole approximation for the electron–photon interaction, since the transition energy is calculated as the difference between the corresponding energy eigenvalues. However, as we have shown in the inset of Fig. 6, this near independence is no longer valid for QDs of large radius, because the Coulomb interaction energy more strongly depends on the quantum state for more separated electrons. Nevertheless, the differences between the transition energies are very small.

6. Summary

In the present paper, we have shown that the artificial helium atom (electron pair in the QD) and the artificial lithium atom (electron triple in the QD) can form bound states with discrete energy spectra, which – for small QDs – are qualitatively similar to those of natural atoms. The conditions of binding obtained in the present paper should be useful in experiments with the QDs. It has been shown that the dipole transition energy for the few-electron artificial atoms is almost independent of the electron–electron interaction. We have found that the order of energy levels substantially changes as a function of the QD radius.

The results of the present paper can be applied to Si/SiO_2 and Ge/SiO_2 spherical QDs as well as to the Si nanocrystals, which are formed in the porous

silicon. We predict that in these nanocrystals the excess electrons can create few-electron bound states with discrete energy spectra and finite binding energies. The energy scale for the created artificial atoms is determined by the depth of the confinement potential. In contrast to the artificial atoms, the characteristic energy scale for the confined excitons is determined by the band gap of the nanocrystal. The radiative transitions between the discrete energy levels of artificial atoms and confined excitons should be clearly distinguished from each other in spectroscopic experiments. To the best of our knowledge, the present work provides the first theoretical results for the ground and excited states of artificial helium and lithium atoms with the finite-barrier confinement potential.

Acknowledgements

This paper is partially supported by the Scientific Research Committee (KBN) under grant No. 2 P03B 05613. The computer calculations were performed at the Academic Computer Center CYFRONET in Kraków (grant KBN/S2000/AGH/050/1998).

References

[1] U. Meirav, M.A. Kastner, S.J. Wind, Phys. Rev. Lett. 65 (1990) 771.
[2] P.A. Maksym, T. Chakraborty, Phys. Rev. Lett. 65 (1990) 108.
[3] M.A. Kastner, Phys. Today 46 (1993) 24.
[4] Q. Ye, R. Tsu, E.H. Nicollian, Phys. Rev. B 44 (1991) 1806.
[5] L. Yue, Y. He, J. Vac. Sci. Technol. B 15 (1997) 1607.
[6] M.A. Olshavsky, A.N. Goldstein, A.P. Alivisatos, J. Am. Chem. Soc. 112 (1990) 9438.
[7] D. Frohlich, M. Haselhoff, K. Reimann, T. Itoh, Solid State Commun. 94 (1995) 189.
[8] T.D. Krauss, F.W. Wise, Phys. Rev. B 55 (1997) 9860.
[9] G.W. Bryant, Phys. Rev. Lett. 59 (1987) 1140.
[10] U. Merkt, J. Huser, M. Wagner, Phys. Rev. B 43 (1991) 7320.
[11] P. Hawrylak, Phys. Rev. Lett. 71 (1993) 3347.
[12] D. Pfannkuche, V. Gudmundsson, P.A. Maksym, Phys. Rev. B 47 (1993) 2244.
[13] M. Macucci, K. Hess, G.J. Iafrate, Phys. Rev. B. 48 (1993) 17 354.
[14] A. Matulis, F.M. Peeters, J. Phys.: Condens. Matter 6 (1994) 7751.
[15] F.M. Peeters, V.A. Schweigert, Phys. Rev. B. 53 (1996) 1468.
[16] M. Fujito, A. Natori, H. Yasunaga, Phys. Rev. B 53 (1996) 9952.
[17] H.-M. Müller, S.E. Koonin, Phys. Rev. B 54 (1996) 14 532.
[18] J.-L. Zhu, Z.Q. Li, J.Z. Yu, K. Ohno, Y. Kawazoe, Phys. Rev. B. 55 (1997) 15 819.
[19] L. Jacak, J. Krasnyj, A. Wójs, Physica B 229 (1997) 270.
[20] C.Y. Fong, B.M. Klein, J.S. Nelson, Modelling Simul. Mater. Sci. Eng. 4 (1996) 433.
[21] G. Fishman, I. Mihalsescu, R. Romestain, Phys. Rev. B 49 (1993) 1464.
[22] B. Delley, E.F. Steigmeier, Appl. Phys. Lett. 67 (1995) 2370.
[23] S. Szafran, J. Adamowski, S. Bednarek, B. Stébé, Mol. Phys. Rep. 21 (1998) 89.
[24] B. Szafran, J. Adamowski, B. Stébé, in: G. Davies, M.H. Nazaré (Eds.), Defects in Semiconductors ICDS-19, Trans Tech Publications Ltd., Switzerland, 1997, p. 1707.
[25] B. Szafran, J. Adamowski, B. Stébé, J. Phys.: Condens. Matter 10 (1998) 7575.
[26] J.C. Slater, Quantum Theory of Atomic Structure, vol. II, McGraw-Hill, New York, 1960.
[27] L. Bányai, S.W. Koch, Semiconductor Quantum Dots, World Scientific, Singapore, 1993.
[28] F. Bloch, Z. Phys. 57 (1929) 545.
[29] W. Kohn, Phys. Rev. 123 (1961) 1242.
[30] J. Adamowski, B. Szafran, S. Bednarek, B. Stébé, Few-Body Systems Suppl. (1998).
[31] S. Tarucha, D.G. Austing, T. Honda, R.J. van der Hage, L.P. Kouwenhoven, Phys. Rev. Lett. 77 (1996) 3613.
[32] B. Szafran, S. Bednarek, J. Adamowski, Acta Phys. Polon. A 94 (1998) 555.
[33] L.E. Brus, J. Chem. Phys. 80 (1984) 4403.
[34] D. Babić, R. Tsu, R.F. Greene, Phys. Rev. B 45 (1992) 14 150.
[35] M. Iwamatsu, M. Fujiwara, N. Happo, K. Horii, J. Phys.: Condens. Matter 9 (1997) 9881.
[36] L. Belkhir, Phys. Rev. B 50 (1994) 8885.
[37] P.A. Maksym, L.D. Hallam, J. Weiss, Physica B 212 (1995) 213.
[38] R.C. Ashoori, H.L. Stormer, J.S. Weiner, L.N. Pfeiffer, K.W. Baldwin, K.W. West, Phys. Rev. Lett. 71 (1993) 613.
[39] H. Drexler, D. Leonard, W. Hansen, J.P. Kotthaus, P.M. Petroff, Phys. Rev. Lett. 73 (1994) 2252.
[40] A.P. Alivisatos, J. Phys. Chem. 100 (1996) 13 226.
[41] M. Haselhoff, H.-J. Weber, Mater. Res. Bull. 30 (1995) 607.
[42] J.C. Slater, Phys. Rev. 36 (1930) 57.
[43] P. Bakshi, D.A. Broido, K. Kempa, Phys. Rev. B 42 (1990) 7416.
[44] F.M. Peeters, Phys. Rev. B 42 (1990) 1486.